ACADEMIC PRESS

Available online at www.sciencedirect.com
SCIENCE DIRECT®

Journal of Catalysis 216 (2003) 32–46

JOURNAL OF CATALYSIS

www.elsevier.com/locate/jcat

The implications of the fundamentals of shape selectivity for the development of catalysts for the petroleum and petrochemical industries

Thomas F. Degnan, Jr.

ExxonMobil Research and Engineering Company, Strategic Research Laboratory, Annandale, NJ 08801, USA

Received 31 July 2002; revised 25 October 2002; accepted 8 November 2002

Abstract

Attempts to explain observations of catalytic selectivity in highly ordered materials with different pore dimensions and different degrees of pore interconnectedness have driven the general theoretical development of shape selectivity in molecular sieves. Fresh theories have emerged with the discovery of new molecular sieves, or as newly found catalytic importance has shifted attention back onto older materials. Highly evolved stochastic and molecular dynamic models are able to accurately represent the primary effects of shape selectivity, yet gaps in our overall understanding still remain. The fundamental concepts underlying shape selectivity have been used very effectively in the development of new catalysts for the petroleum and petrochemical industries. While the focus has recently moved to the more extensive application of shape-selective catalysis to fine chemicals, significant advances in the form of new processes and applications of new materials continue to be made in petroleum refining and commodity petrochemical industries. As the concept of shape-selective catalysis in molecular sieves nears its forty-third anniversary, several of its theoretical bases remain topics of intense study.

Keywords: Shape selectivity; Molecular sieves; Zeolites

1. Introduction

Few concepts have had a greater impact on the design and development of novel catalytic processes for petroleum refining and petrochemical manufacture than that of shape-selective catalysis. First proposed by Paul Weisz in 1960, the concept of shape selectivity in molecular sieves was actually rooted in the workings of enzymatic catalysts [1–3]. Today, the concept is the basis for at least 17 commercial processes with annual hydrocarbon throughputs in excess of 70 million metric tons per year. Shape selectivity in molecular sieves remains a subject of intense study. The last decade has produced over 600 papers and more than 300 US patents on the subject. Prominent reviews include Refs. [4–19]. Highly personalized and insightful papers by Weisz and co-workers [1–5] and Csicsery [6–10] are particularly relevant. The initial concepts proposed by Weisz and extended by Csicsery have provided the foundation for much of the theory upon which shape-selective catalysis is built.

2. Classical theories of shape selectivity

There are presently three acknowledged and five less widely accepted theories of shape selectivity in molecular sieves. Four of these theories relate to mass transfer within the pores of the molecular sieve, while four others concern limitations in the transition state either on the surface or within the pores. Shape-selective reactions governed by mass transfer within the molecular sieve involve what Weisz has entitled "Configurational Diffusion" [1]. Configurational diffusion occurs when the diameter of the molecules approaches the structural dimensions of the intracrystalline pores.

Reactant shape selectivity (RSS) distinguishes between competing reactants on the basis of size exclusion at or very near the pore mouth [4]. Only a fraction of the reactants can easily reach the internal active sites due to the size of the pore openings. Clearly, this type of selectivity depends on the geometry at the entrance to the pore and on the intrapore diffusional characteristics of the reacting molecules. The classic example, described by Weisz [4], is the Linde 5A catalyzed dehydration of *n*-butanol without reacting isobutanol. A more useful example is the exclusion of multiply branched paraffins in the selective catalytic

E-mail address: thomas_f_degnan@exxonmobil.com.

0021-9517/03/$ – see front matter
doi:10.1016/S0021-9517(02)00105-7

"dewaxing" of waxy distillates and lube fractions over ZSM-5 [20].

Product shape selectivity (PSS) refers to the situation where the pore diameter effectively discriminates between products exiting the pores on the basis of the size of the product molecules [4]. Thus, products that may be formed in the larger intersections between several pores can diffuse out of the molecular sieve only if they are small enough in relation to the diameter of the pores. Examples of PSS include selective toluene disproportionation to produce *para*-xylene and the methanol-to-gasoline (MTG) reaction where the largest alkylated aromatics formed are tetramethylbenzenes [21].

Transition-state selectivity (TSS) pertains to reactions where the geometry of the pore around the active sites imposes steric constraints on the transition state [7]. Thus, the effective diameter of the pores or the intersections strongly inhibits the formation of unstable transition states or reaction intermediates. Useful examples of TSS include the inhibition of coke formation within ZSM-5 (MFI) crystals and the cracking of paraffins within the MFI pores [22]. In the latter case, pore size constraints prevent the formation of the transition state needed for hydrogen transfer thereby conserving the light olefins produced by cracking from being transformed into corresponding, lower octane number, light paraffins.

The three well-accepted types of shape selectivity are depicted graphically in Fig. 1.

Still subject to vigorous debate are the theories of inverse shape selectivity, molecular traffic control, pore mouth–key–lock shape selectivity, the "Window Effect," and the "Nest Effect."

Inverse shape selectivity (ISS) attempts to explain the preferential adsorption of bulkier vs less bulky molecules within the pores of some sieves [23]. The theory is based primarily on attempts to explain experimental data with computational simulations, which use energetic contribution theory for the molecules and calculated force fields within the molecular sieve. The specific situations studied relate to the stabilization of polymethylparaffins vs linear or monomethylparaffins. The results of Santilli et al. have recently been reexamined by Smit and co-workers [24,25], who concluded that the preferential adsorption of bulky molecules occurs only in a narrow region of the adsorption isotherm where high loadings allow for preferential siting and close packed arrangement of the branched molecules at the intersections of the pores.

Molecular traffic control (MTC) is specific to molecular sieves where two or more pore systems with different diameters or tortuosities intersect [26,27]. In the case of two intersecting pore systems, one participating molecular species can diffuse readily in both pore systems while the other can only move through one of the systems. Thus, reactants can enter one type of pore, be converted within the sieve, and diffuse out through another type of pore. In cases where a smaller or more tortuous pore intersects larger or straighter pores, smaller reactants are able to enter through one pathway and react at the intersection to form larger molecules. The product molecules are able to exit through another set of larger pores, effectively precluding counterdiffusion and improving the overall diffusivity of both reactants and products. It is possible that molecular traffic control may be manifested in ZSM-5 catalyzed toluene disproportionation [17], but for reasons described below this is difficult to confirm experimentally.

Pore mouth and key–lock selectivity (PMKLS) pertains specifically to the interactions of normal and branched

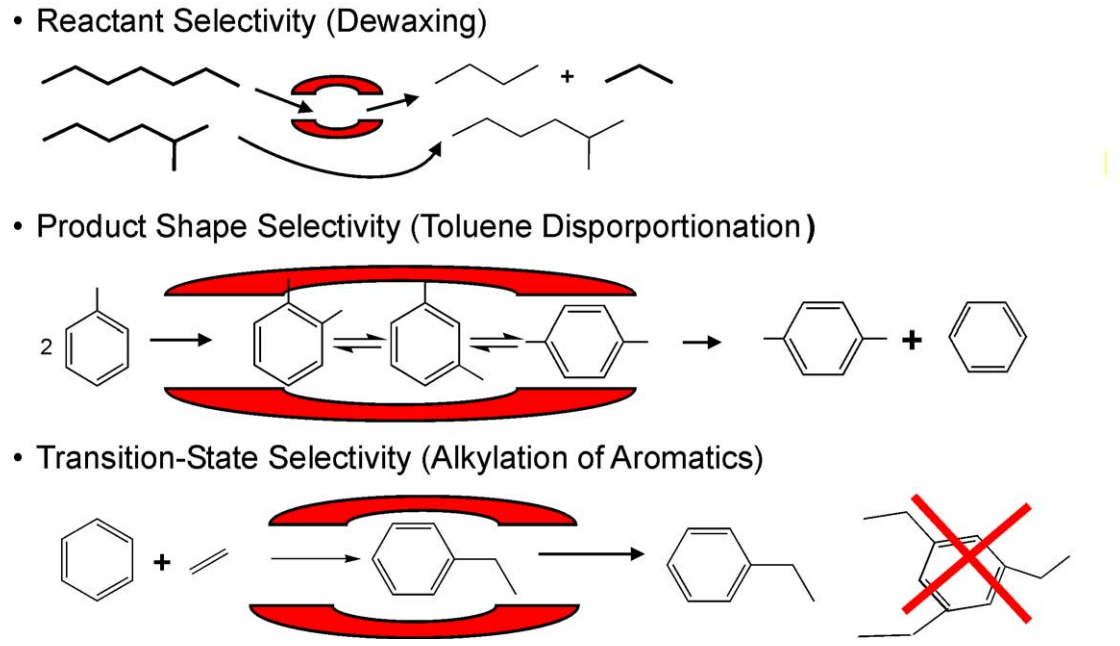

Fig. 1. Examples of classical shape selectivity from the literature.

paraffins in unidimensional, nonintersecting medium-pore molecular sieves [28–36]. The theory has been proposed to explain the highly selective nature of these molecular sieves for the hydroisomerization of longer chain normal paraffins, which is important in changing the cold flow properties of transportation fuels and lubricants. A high degree of 2-methyl branching in the product for these reactions is explained by the selective adsorption of the *n*-paraffin onto the external surface and at the pore mouth. Methyl branching occurs only on that part of the chain located immediately outside of the pore. In key–lock adsorptions, the opposite ends of long paraffins adsorb into two different pores leading to branching near the central C atom. Fig. 2a shows the favorable adsorption configurations of C_{21} molecules in ZSM-22 (TON) [36].

The "Window Effect" (WE) attempts to explain large "up and down" variations in the diffusivity of *n*-paraffins with increasing carbon number [37–42], Fig. 2b. The effect, first noted in zeolite-T and chabazite (CHA), has been the subject of numerous computational and experimental studies. The effect has been rarely found except in this specific family of zeolites. The Window Effect has recently been reexamined by Schenk et al. [43], who have attempted to reconcile the disparate observations in terms of selective adsorption and sorbate packing in the larger intersections.

The "Nest Effect" (NE) has been proposed to account for shape selectivity changes derived from the presence of non-shape-selective catalytically active sites on the external surface of the crystals [44,45], Fig. 2c. This theory also postulates that acid sites located in cavities formed by the terminus of the pore at the surface can provide for a different type of shape selectivity than that found within the pore. An example of the Nest Effect is the synthesis of ethylbenzene over MWW zeolites [46].

In contrast to the shape selectivity imposed by the physical dimensions or configuration of the pores, there is also the concept of secondary shape selectivity [47,48]. Secondary shape selectivity involves the constraints associated with the presence within the pores of strongly adsorbed species other than reactants or products. For example, reactants can compete with each other based on their relative rates of diffusion. A larger reactant can reduce the diffusivity or sterically inhibit the adsorption of a smaller co-reactant.

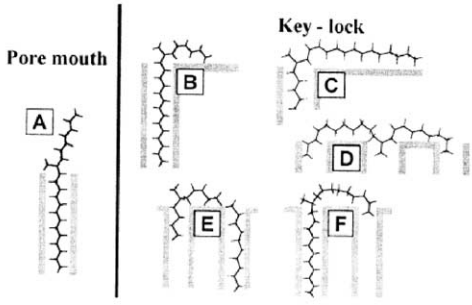

(a) Pore Mouth and Key Lock Mechanisms [36]

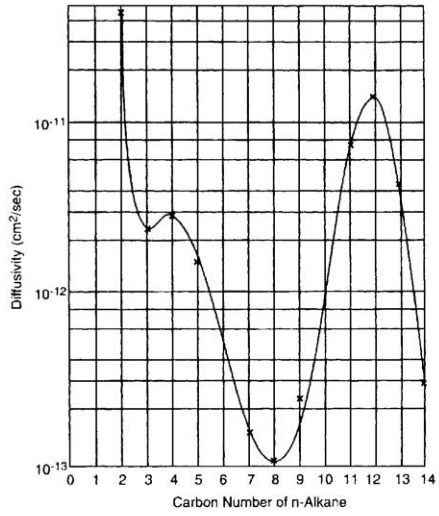

(b) The Window Effect [37]

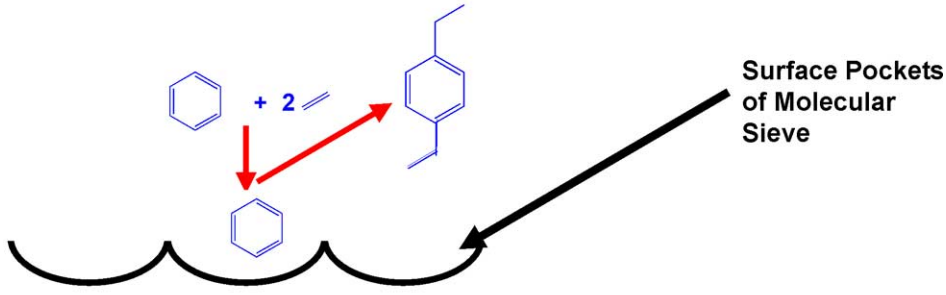

(c) The Nest Effect [45]

Fig. 2. (a) Pore mouth and key–lock mechanisms as illustrated by the adsorption of C_{21} molecules into the pores of ZSM-22, (b) the window effect, and (c) the nest effect.

3. Discriminating among various types of shape selectivity

In many cases it has been difficult to determine whether more than one type of shape selectivity is operating. The impact of molecular traffic control (MTC) for example, is to increase the diffusivity by a factor of two over what might be assumed without the theory [49]. This change is small in comparison with the four- to six-order-of-magnitude change in diffusivity that is measured in shape-selective reactions [2]. It has also been difficult to discriminate between product selectivity shape (PSS) and transition-state selectivity (TSS), and it is possible that both are operative in many cases. Discriminating between the two types requires a study of the reaction kinetics using different crystallite sizes. While conceptually attractive, this strategy is empirically very difficult since molecular sieves are frequently synthesized with a distribution of crystallite sizes. Also, it is often difficult to maintain, as constant, the density of the active sites while varying crystallite size. Finally, several of the theories, such as inverse shape selectivity (ISS), have been forced to rely upon computational simulations to substantiate their existence [23]. Different assumptions used in developing the models have led to vastly different interpretations.

4. The impact of the external surface on shape selectivity

The development of the theories of pore mouth and key–lock selectivity (PMKLS) and the "Nest Effect" (NE) recognize the importance of the external surface of the molecular sieve. In fact, the full impact of the external surface on catalytic activity and selectivity was not truly appreciated until the mid-1980s [50]. Because the crystals have internal "surface areas" of several hundred square meters per gram and typical external surface areas of no more than 10 m^2 per gram, the relative contribution of the external surface to activity and selectivity was historically considered to be negligible. Moreover, it was not clear whether the active sites on the external surface were similar in strength to those located in the electron rich interior of the crystal.

Two developments changed this paradigm. The first was the realization that the inorganic oxides used as binder systems could participate in isomorphous substitution of framework species especially adjacent to the external surface. Shihabi et al. showed that in high-silica zeolites such as ZSM-5, aluminum derived from alumina or silica–alumina binders substituted for silicon or displaced the hydroxyl nests that characterized the framework voids near the external surface of the molecular sieve [51]. Intracrystalline diffusion of aluminum from outside the crystal occurred at elevated temperatures, especially in the presence of polar compounds such as water and methanol. Detrital aluminum generated by steaming could be reinserted under milder conditions. The second development that changed this paradigm was the discovery of synthesis methods that produced very small crystals [52–55]. This increased the relative contribution of the external surface area while reducing the effective diffusion path length.

In situations where reactants are subject to substantial intracrystalline diffusion limitations, the surface contributions to the overall activity may be commensurate with the contributions of all of the internal sites. Even more dramatic are the effects on catalytic selectivity [56]. Reactant and product shape selectivity can be markedly changed as a result of even a small number of non-shape-selective active sites on the surface.

5. Application of advanced techniques to understanding the fundamentals of shape selectivity

Significant strides in understanding and utilizing shape selectivity in catalyst design and development during the past 20 years have resulted from the combination of (a) computational simulations [57], (b) vastly improved materials characterization capabilities [58], and (c) meticulous use of model compound studies [59]. Three studies, one in each of these areas, are profiled to demonstrate the degree of understanding provided by what may eventually be considered classical analyses of shape selectivity. The cases were selected to exemplify the importance of each approach. They were also selected to highlight gaps in our understanding of particular aspects of shape selectivity. It will be shown that insights drawn from these fundamental studies can be used collectively in designing a highly selective catalyst for the production of *para*-xylene.

6. Computational studies of shape selectivity—the synthesis of cumene

Cumene is produced by the alkylation of benzene with propylene over solid acid catalysts. Recent advances have focused on the replacement of $AlCl_3$ and solid phosphoric acid catalysts with high-silica zeolites. The advantages of using zeolitic catalysts are in significantly higher cumene yields and purity as well as longer cycle lengths [6]. Production of *n*-propylbenzene and propylene oligomers is significantly reduced over certain large-pore molecular sieves. This is shown in Table 1, where the product selectivities of Beta (BEA), faujasite (FAU), mordenite (MOR), ZSM-12 (MTW), and MCM-22-type (MWW) for the propylene alkylation of benzene [60] are compared. By comparison, solid phosphoric acid catalysts typically produce 4 to 5 wt% of highly undesirable polyisopropylbenzenes. In commercial operations where propylene conversions are typically higher than shown in this table, MWW actually has the lowest selectivity for propylene oligomerization and for producing

Table 1
Comparison of the catalytic selectivities of zeolite Beta (BEA), mordenite (MOR), ERB-1 (MWW), USY (FAU), and ZSM-12 (MTW) in cumene synthesis (150 °C, 3 MPa, benzene/propylene = 7:1 (molar)) (from Ref. [60])

	BEA	MOR	MWW	USY	MTW
Propylene conversion	93.0	92.1	95.4	92.0	95.1
Products (wt%)					
Oligomers	0.1	0.5	0.3	0.4	1.0
n-Propylbenzene, ppm	190	107	277	140	406
Cumene	93.3	86.6	90.7	77.6	94.3
Diisopropylbenzene	6.6	12.8	8.8	21.5	4.6
DIPB isomers, %					
ortho-	1.1	1.1	1.7	19.5	2.2
meta-	63.6	62.0	45.5	37.0	29.7
para-	35.3	36.9	54.8	43.5	68.1

Thermodynamic equilibrium for DIPB's: *ortho*-/*meta*-/*para*- = 9.9/58.1/32.0.

trace amounts of ethylbenzene among the zeolites shown in Table 1 [46].

Attempts to understand the improved selectivity produced a series of elegant computational molecular dynamics studies comparing the diffusion barriers for cumene in different zeolites [60–63]. This was one of the first series of studies where the energy plots were generated along with visual plots of the molecules passing through the pores. The molecular dynamics calculations of the diffusion energy barriers (Table 2) were able to explain the vastly different selectivities observed for the diisopropylbenzene isomers. Higher diffusion energy barriers computed for *ortho*-DIPB in BEA, MOR, and MTW accounted for the low selectivity of these isomers as measured in the catalytic test. The computations also confirmed why the *meta*-/*para*-DIPB ratio was able to approach equilibrium in the larger pore BEA and MOR zeolites.

The initial computational studies were not successful in explaining the unique selectivity and activity of the MWW molecular sieve. MWW consists of two independent pore systems, both of which have 10-member ring apertures. One system consists of sinusoidal pores parallel to the 010 plane and the other by large supercages that are 1.76 nm long and 0.71 nm in diameter, interconnected by slightly elliptical apertures as shown in Fig. 3 [64]. The large supercages within the zeolite are only accessible through 10-member ring pores. The computed energy barriers for cumene diffusion in the 10-member ring pores of MWW were so high as to predict that the zeolite should have little or no activity for cumene synthesis. Yet, the experimental data showed MWW to be comparable to or better than the other large-pore zeolites both in benzene alkylation activity and in cumene selectivity.

Table 2
Computed diffusion energy barriers in six different zeolites (kJ/mol) (from Ref. [60])

	Cumene	*o*-DIPB	*m*-DIPB	*p*-DIPB
Medium pore zeolites				
MWW	233.2	No diffusion	620	331.5
MFI	77.9	No diffusion	439	63.6
Large pore zeolites				
BEA	20.9	223.5	57.3	14.2
MOR	13.8	95.0	51.9	11.7
FAU	26.4	71.2	16.7	10.1
MTW	21.3	276.3	64	19.3

Pore system containing the supercages. The energy barrier for diffusion of cumene in the sinusoidal pores is 377 kJ/mol.

The explanation for this unusual behavior resulted from an analysis of the morphology of the MWW crystal and an attempt to understand how the molecular sieve is formed. The crystals form as thin lamellae with a significant amount of external surface area. The lamellae contain the sinusoidal 10-member ring pore system, but the surface is composed of 0.71-nm-deep by 0.71-nm-diameter pockets that form as hemisupercages resulting from the truncation of the supercages at the surface.

The computational analysis by Perego et al. showed that the reaction occurs on the surface without diffusion barriers, but under steric control [63]. Calculations of the energetics and location of diisopropylbenzenes and cumene in the surface pockets further support this hypothesis. Molecules are determined to be strongly adsorbed, leading to the conclusion that product molecules can be accommodated sterically within the pockets.

The surface contribution to the overall intrinsic activity of the MWW-type zeolite was confirmed experimentally by selectively poisoning the surface using collidine in a study that examined the liquid phase alkylation of benzene with ethylene [65]. Collidine is highly basic and has a molecular diameter of 0.71 nm, which fits exactly within the surface pockets. Its size prohibits it from being adsorbed within the 10-member ring pores. The correspondence between the amount of collidine required to poison the 20% of sites computed to remain on the surface and the ability for this level of collidine to completely eliminate all alkylation activity confirmed that the catalytic activity was entirely attributable to the surface sites.

While the surface pockets lack any diffusion barriers, they do exhibit a pronounced and very unique shape selectivity for *ortho*-dialkylbenzene at low conversions. This is likely due to steric constraints associated with the preferred location of the alkylbenzene and the ability for the olefin to access the active site. The *ortho*-selectivity of MWW-type molecular sieves in aromatic alkylation reactions has not been explained via computational modeling. Nor has modeling been able to explain MWW's unique low selectivity for olefin oligomerization.

The study by Perego et al. also attempted to use binding energy computations to explain the selectivity differences in diisopropylbenzene production [63]. Since DIPB's are formed via sequential reactions, it is logical to expect that molecular sieves that adsorb cumene more strongly would have the highest selectivity for DIPB. Computations showed very good agreement between cumene binding energies and DIPB yield.

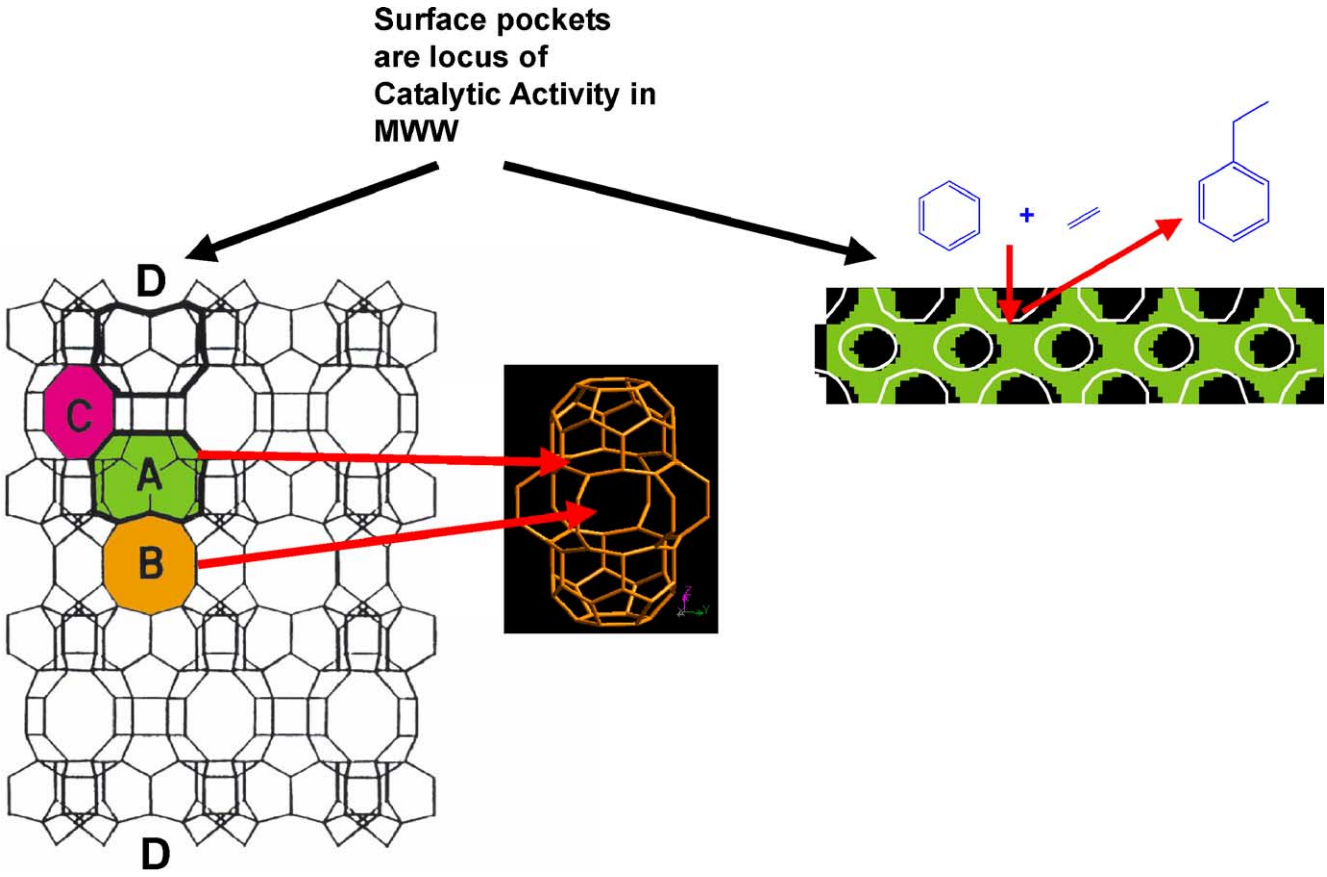

Fig. 3. Schematic of MWW (MCM-22). MCM-22 has unique structural features: (i) 12-ring cavity (A) accessible through a 10-ring aperture (B), (ii) 10-ring channel system (C), and (iii) 12-R surface pockets (D).

This example demonstrated two major points in understanding shape selectivity. The first is the power of computational modeling coupled with experimental confirmation of the hypotheses drawn from the model in explaining shape selectivity. Specifically, this study showed the importance of both product shape selectivity (PSS) and transition shape selectivity (TSS) in governing the isomer distribution of dialkylbenzenes in large pore molecular sieves. It also showed the significance of surface activity and surface morphology (i.e., "The Nest Effect") on shape selectivity in small crystal or lamellar molecular sieves such as MWW.

Similar computational studies have been carried out by Horsley in the identification of mordenite (MOR) as the most selective molecular sieve for the synthesis of 2,6-diisopropylnaphthalene [66] and by Moorwier et al. in their attempts to explain the unique selectivity of ferrierite (FER) in the skeletal isomerization of butene [67].

7. Model compound studies of shape selectivity—cracking of C6–C9 paraffins

Aside from complete steric exclusion of either the transition state or the reactant itself, shape selectivity is dominated by the competitive diffusion rates of reactants and products. Attempts to directly define the shape selectivity produced by specific frameworks and crystal sizes have suffered from imprecise measurements of diffusion coefficients and a realization that the hard body models are not accurate. This is particularly true at elevated temperatures, characteristic of most catalytic reaction conditions, where considerable amount of molecular sieve framework "flexing" occurs and where translational and vibrational energetics are sufficient to modify the assumed effective diameter of the diffusing molecule [68].

In an elegant study, Haag et al. [69] attempted to discriminate between transport induced shape selectivity (i.e., RSS and PSS) and transition-state selectivity (TSS) by applying classic transport models of diffusion and reaction to a series of MFI crystals of distinctly different sizes and activities. The crystals used in this study were carefully prepared to target specific SiO_2/Al_2O_3 ratios and crystal sizes. While Al zoning is a concern among large-crystal, high-silica zeolites such as MFI, XPS analysis confirmed uniform Al distribution even in the larger crystals. The study involved an analysis of the individual cracking rate constants of a set of pure normal and branched C_6 through C_9 paraffins and olefins at atmospheric pressure and 538 °C. The partial pressure of the hydrocarbons was varied to establish the first-order cracking rate constant for each model hydrocarbon. By comparing the observed rate constants for different sized

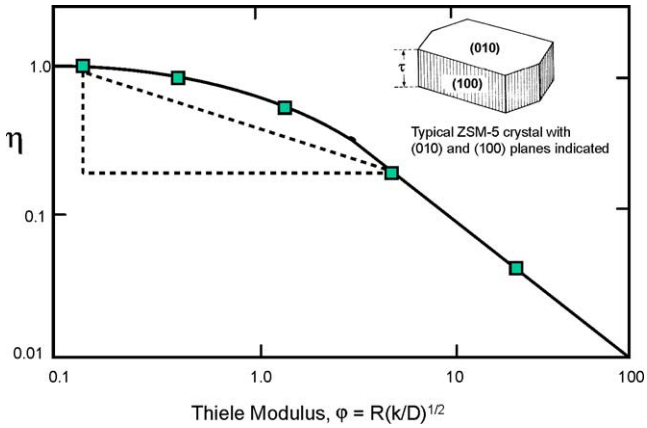

Fig. 4. Triangulation method used in establishing relative effectiveness factors [69].

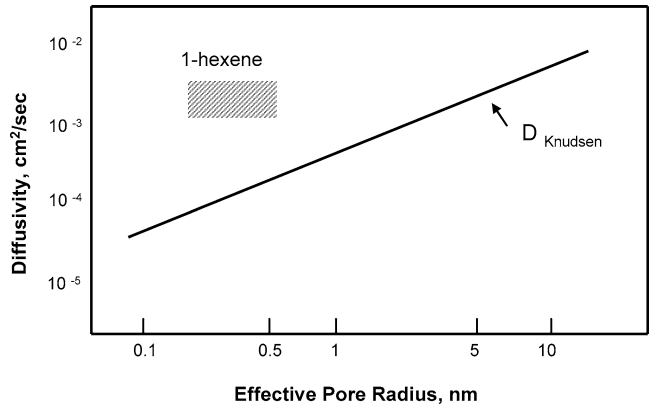

Fig. 5. Knudsen diffusivity as a function of effective pore radius and observed diffusivities for 1-hexene [69].

crystals of equivalent activities, Haag et al. were able to determine both the intrinsic rate constants, k_{int}, and the effectiveness factor, η, of each hydrocarbon for each crystal size, R. Assuming a flat plate geometry for the MFI crystals, where $R = 1/2$, the thickness of the plate, the authors were able to use the classical effectiveness factor function,

$$\eta = (\tanh\varphi)/\varphi,$$

where the modulus φ is defined as $\varphi = R(k_{\text{int}}/D)^{0.5}$, to establish the intracrystalline diffusion coefficients, D, for each hydrocarbon under the reaction conditions. The flat plate geometry was assumed because the crystal habit of larger MFI crystals is typically a platelet in which the dominant diffusion path is through the shorter straight channels perpendicular to and into the (010) surface of the platelet-like crystals (Fig. 4). For smaller MFI crystals, the crystal habit is more spherical, and the assumption of flat plate geometry introduces some error, although this is likely small since the relationship between the effectiveness factor and the modulus is less a function of geometry as the modulus gets smaller.

Haag et al. used a clever triangulation technique and the effectiveness factor curve to locate precisely where they were on the curve for each crystal. By determining the value of R for two crystals from scanning electron microscopy (SEM) and transmission electron microscopy (TEM) measurements and measuring the observed rate constant for the first-order paraffin or olefin cracking reaction over the same two crystals under identical reaction conditions, they were able to determine two ratios, η_1/η_2 and R_1/R_2. The values of these two ratios correspond uniquely to the length of the vertices of a triangle that intersects the effectiveness factor plot at the point where the vertices connect to the hypotenuse (Fig. 4). Knowing the value of the modulus, φ, the radius, R, and the intrinsic cracking rate constant, k_{int}, permits the direct calculation of D, the intracrystalline diffusion coefficient.

The study conclusively showed that there was no diffusion inhibition in MFI for normal and monomethyl paraffins, e.g., 3-methylpentane, but that the diffusivities of 2,2-dimethylbutane and 2,2-dimethylheptane were strongly influenced by crystallite size. The cracking of dimethyl paraffins was invariably diffusion limited irrespective of the MFI crystallite size. Olefins had cracking rate constants approximately 20 times greater than those of the corresponding paraffins. This increased the value of the modulus and moved the reaction into the diffusion-limited regime for all but the normal olefins.

A comparative analysis of the relative rates of diffusion and cracking of singly branched and normal paraffins showed that transport effects could not explain the measured rate constants. Instead, the authors demonstrated that steric constraints (TSS) limited the rate of formation of a larger methyl paraffin/carbenium ion reaction complex.

Surprisingly, the actual diffusivities of the hydrocarbons measured at 538 °C markedly exceeded the Knudsen diffusivities, Fig. 5 [70]. The Knudsen model, which applies to dilute gas phase diffusivities in narrow pores, assumes that interactions between molecules and the pore walls are inelastic and that molecules have no memory of the angle of incidence. Haag et al. speculated that the reasons behind the significantly higher than expected diffusivity lie in the inappropriate assumptions associated with using Knudsen diffusion as a model. The assumption of Knudsen diffusion may break down for linear molecules within the confines of the molecular sieve pores where the tendency of the zeolite to concentrate molecules increases the probability of collisions with other molecules versus collisions with the zeolite walls. Nor does Fickian diffusion explain the higher than expected diffusivities. The diffusion coefficients for C_6–C_9 linear paraffins and olefins measured in this study exceed those determined from room temperature uptake and NMR studies of the same paraffins in MFI molecular sieves [71,72]. Whether the enhanced diffusivities are related to the significantly higher temperatures used in the study or to some other effect has not been clearly established. In the case of molecular sieves, a strong temperature dependence of the diffusion coefficient has been interpreted in terms of “activated diffusion” [5].

Similar studies, directed toward extracting fundamental transport properties by measurement of reaction rate constants over a well-defined set of materials comprising different size crystals with narrow crystal size distributions and well-controlled active site concentrations, are rare. Two other examples are the well-constructed studies examining xylene isomerization [73,74] and toluene disproportionation in MFI molecular sieves [75,76]. In each of these studies the effect of the external surface on altering *para*-selectivity has been ignored. Recent studies by Jones and Davis [77] and Niwa et al. [78] have attempted to address the impact of non-shape-selective reactions occurring on the crystal surface and their impact on xylene isomerization and toluene disproportionation.

We will consider toluene disporportionation over surface modified zeolites in more detail below. Catalytic studies involving specially prepared zeolite crystals with precisely controlled zeolitic composition and crystal size are extremely important in establishing the relative significance of mass transport and steric constraints in catalytic shape selectivity under realistic reaction conditions. They are immensely important in establishing fundamental parameters for designing catalysts for commercially important shape selective reactions.

Additional insight into the shape-selective properties can be derived from model compound tests that are directed toward eliciting characteristics of the pore structure of molecular sieves. This is especially important for those materials whose structure has not been resolved. These tests typically involve the comparison of the rates of reaction of two model compounds or an analysis of the product selectivities from the conversion of a single model compound. Examples include paraffin cracking, e.g., the Constraint Index (CI) [79] and Spaciousness Index tests [80], hydroisomerization of longer chain paraffins [81], aromatic transformations [82], conversion of alkylnaphthenes and polycyclic naphthenes [83], and isomerization of alkylnaphthalenes [84]. The use of the Constraint Index to determine the pore size and structure has recently been challenged [85]. This study by Zones and Harris suggests that some zeolite structures can produce anomalous Constraint Index values. It has become clear that catalytic characterization with model compounds must be supplemented by structural characterization of the molecular sieve to get an adequate understanding of how shape selectivity influences the targeted reaction.

8. Structural characterization of shape selectivity—X-ray diffraction, high-resolution electron microscopy, and magic angle spinning NMR

The three most important methods for characterizing the structure and composition of molecular sieves are arguably diffractometry (X-ray and electron), high-resolution electron microscopy (TEM, SEM, and HREM), and magic angle spinning nuclear magnetic resonance (MAS-NMR). Atomic force microscopy (AFM) has also afforded some unique perspectives, but is not as widely used for characterizing molecular sieves as the other forms of microscopy because it is specifically tailored to flat surfaces rather than particles. X-ray diffraction can be used to determine the presence of polymorphs as in the case of zeolite Beta (BEA), while high-resolution electron microscopy can distinguish between crystallite size and particle size, and also identify the presence of intergrowths or crystal imperfections where X-ray diffraction is not helpful. MAS-NMR is useful in determining the ordering of framework atoms such as Si and Al. When used with a probe such as Xe^{129} the technique can accurately identify and quantify the concentration of large ions and coke within the pores. An attempt to summarize recent advances in these characterization techniques and their application to molecular sieves is outside of the scope of this paper. However, it is important to highlight some of the more significant studies that illustrate the critical need for these techniques in understanding reaction shape selectivity.

One of the earliest studies of the combined application of HREM and MAS-NMR to characterize shape selective molecular sieves by Thomas et al. [86] remains one of the best in demonstrating the value of these techniques. The study examined, in detail, samples of ZSM-5 (MFI) and ZSM-11 (MEL). Comparative studies of MFI and MEL structures previously demonstrated differences in transition-state selectivity (TSS) derived from the differences in the effective diameter of the intersection between the dual straight channels of the MEL framework and the sinusoidal and straight pore intersection in the MFI framework.

For example, Derouane et al. examined methanol-to-gasoline and alkylation of para-xylene with methanol reactions using a series of specially prepared MFI and MEL zeolites consisting of different crystal sizes within a limited range of Al contents and with identical crystal sizes [87]. They found that the MEL structure produced more C_9 aromatics in the MTG reaction and that it had a greater alkylation activity in the *para*-xylene–methanol reaction at equivalent acid site concentrations. Both results suggest the presence of a larger effective diameter within the MEL crystal. For this reason it was important to determine whether intergrowths of orthorhombic MFI and tetragonal MEL exist. The analysis of MFI samples did show the coexistence of MEL. However, Thomas et al. were unable to identify superlattice repeats proposed by other researchers. They did not attempt to correlate diffusive properties with the presence of the intergrowths.

The influence of crystal defects and intergrowths on shape selectivity has received very little attention. Recent advances in both HREM and MAS-NMR have incorporated capabilities for examining catalysts in contact with reactants under actual reaction conditions as well as for examining the exact location of metals and metal oxide clusters within zeolites [88]. These innovations should significantly improve our ability to examine the molecular dynamics within the pores of molecular sieve catalysts and further our under-

standing of the roles of mass transfer and steric constraints within the pores.

Significant advances in the use of HREM to elucidate the structures of micro- and mesoporous materials have been described in reviews by Terasaki et al. [89] and in publications by Terasaki's collaborators, Wagner [90], Inagaki [91], and Carlsson [92]. Their work has produced several new approaches to solving the structures of porous materials using both electron diffraction (ED) and HREM. They used these methods in the structural analysis of SSZ-48 and in the 3-D structural analysis of mesoporous MCM-48 [89].

HREM has also been instrumental in direct imaging of pores and cages of microporous and mesoporous materials. HREM produces two-dimensional projections that can be then transformed into three-dimensional images by inverse Fourier transformations of the images. Sakamoto et al. [93] have used this technique to resolve the cage and pore structures of three mesoporous materials (SBA-1, SBA-6, and SBA-16) and show that these structures consist of highly ordered dual micro- and mesopores.

Finally, HREM has been used in detailed analysis of surface structure. For example, Ohsuna et al. [94] used HREM to examine the termination structure of the surface of zeolite L. They compared the HREM images with simulated images derived from ideal models and determined that the zeolite is terminated with double six-member rings on the (001) surface and with cancrinite cages on the (100) and (110) surfaces. The application of HREM in combination with specific catalytic studies to evaluate the impact of surface pockets and active site location on shape selectivity remains to be exploited.

Atomic force microscopy (AFM), combined with HREM and modeling has provided important insights into the formation of intergrowths and the role of defects in crystallization. Atomic resolution of zeolite surfaces in the absence and presence of hydrocarbon adsorbates has revealed surface structure [95]. These studies have also provided insights into the mode of interaction of structure directing agents leading to an improved understanding of molecular "templating" [96]. Knowledge gained from such AFM studies has been used in the preparation of shape-selective membranes [97].

Advances in magic angle spinning nuclear magnetic resonance (MAS-NMR) have been equally impressive. MAS-NMR is used in the two-dimensional resolution of framework structures [98]. NMR resonances can be assigned to specific T-sites in proposed framework structures through correlations obtained from quadrupolar coupling constants and isotropic chemical shifts. MAS-NMR has been extended to assess the specific location of hydrocarbon adsorbents within the pores. For example, Morell et al. [99] have used the technique to examine the location of *n*-hexane in the pores of MFI at 180 K and to confirm force field calculations showing that the molecules are located in the straight and sinusoidal channels, leaving the intersections unoccupied. The logical extension of this technique is the use of MAS-NMR under reaction conditions to provide insight into the preferred host-guest structure. Already MAS-NMR can be used to study slow molecular motions and exchange processes within zeolites [100]. The technique has been invaluable in quantitation and location specification of catalytically active framework Al in zeolites, where it has been able to identify as many as four separate aluminum environments [101].

Advances in X-ray diffraction of molecular sieves have mainly concentrated on structure resolution. The combination of powder diffraction analysis and crystal chemical information with powerful new computational algorithms has greatly accelerated the solution of complex structures [102]. This has been particularly true in the application of the FOCUS method to solve new structures, which range in complexity. The FOCUS method combines Fourier recycling with specialized topology searches to solve the structures of three-dimensional four-connected frameworks [103,104].

Alone or in combination with each other, these techniques provide powerful insights needed to design working catalysts.

9. Selective toluene disproportionation—an example of catalyst design using shape-selective concepts

Selective toluene disproportionation (STDP) catalyzed by MFI-type molecular sieves is an excellent example of catalyst design that exploits product shape selectivity (PSS) and transition-state selectivity (TSS) and attempts to minimize the effects of surface activity to maximize *para*-xylene production. More than 30 years after their discovery, MFI-type zeolites remain the preferred basis for STDP catalysts because of their low selectivity for forming tri- and tetramethylbenzene and their relatively high activity for disproportionation. The development of a commercial STDP catalyst drew upon much of the knowledge derived from the aforementioned studies of shape selectivity. To produce an optimal catalyst required a thorough application of HREM, X-ray diffraction and MAS-NMR characterization techniques and extensive evaluation of many methods for modifying both the diffusion characteristics and the number of active sites on the surface of an MFI crystal.

The fundamental strategies for designing the STDP catalyst are outlined in the reviews by Weisz and by Olson and Haag [4,75]. The toluene disproportionation reaction is shown in Fig. 6.

In conventional toluene disproportionation, an equilibrium mixture of xylenes is expected. *para*-Xylene should rapidly equilibrate with the other two isomers since the intrinsic isomerization rate constant, k_I, is normally at least an order of magnitude larger than k_D, the intrinsic disproportionation rate constant. In fact, Olson and Haag found that $(k_I/k_D)_{intrinsic}$ was greater than 7000 for MFI molecular sieves. The objective of STDP is to use shape selectivity to direct the primary product to be highly *para*-selective and

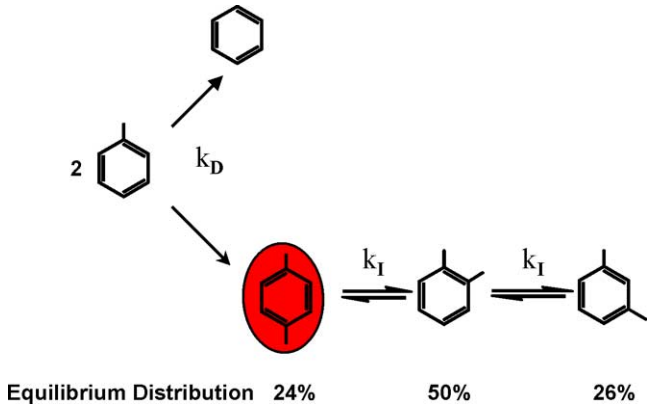

Fig. 6. Toluene disproportionation reaction.

to inhibit the subsequent isomerization of the primary *para*-xylene product.

Olson and Haag established the following basic design criteria for high *para*-xylene as the primary product,

$$D_{p\text{-}} \gg D_{m\text{-},o\text{-}},$$
$$k_I \gg D_{m\text{-},o\text{-}}/R^2,$$
$$k_D \ll D_T/R^2,$$

where $D_{p\text{-}}$ is the diffusivity of *para*-xylene, $D_{m\text{-},o\text{-}}$ is the diffusivity of *meta*- and *ortho*-xylene, D_T is the diffusivity of toluene, R is the radius of the crystal. To minimize secondary isomerization, they postulated that $(k_I/k_D)_{observed}$ must be significantly less than unity, where

$$(k_I/k_D)_{observed} = (h_I/h_D)(k_I/k_D)_{intrinsic} x(\eta_I/\eta_D).$$

Here, η_I is the effectiveness factor of the xylene isomerization reaction, and η_D is the effectiveness factor of the toluene disproportionation reaction. According to Haag and Olson, $D_{p\text{-}}/D_{o\text{-}} > 10^3$ and $D_T \sim D_{o\text{-}}$ ($D_{o\text{-}} \sim D_{m\text{-}}$). Thus, for larger values of the modulus φ (i.e., larger R), $\eta_I/\eta_D < 10^{-3}$ and $(k_I/k_D)_{observed}$ can approach unity. Under these conditions the catalyst can produce *para*-xylene far in excess of equilibrium.

In addition to confirming the predominance of product shape selectivity by varying the crystal size and number of active sites, the Haag et al. study also examined the effects of selectively modifying the diffusion properties through selective incorporation of phosphorus, magnesium, boron, silicon, antimony, and coke. Ultimately, it was determined that the deposition of coke on the exterior of the MFI molecular sieve was preferred since it increased the diffusion path length and covered all of the nonselective external sites without affecting the number of sites internal to the crystal, Fig. 7. Coke can be uniformly deposited by decomposition of monocyclic aromatic compounds at elevated temperatures over MFI catalysts. The deposition of coke and its influence on the acidity and shape selectivity of a broad range of zeolites, including MFI-type zeolites, are the subject of a large number of studies by Guisnet and co-workers [105–108]. The studies of Guisnet and co-workers also include analyses of coke distribution and coke compositional variation in zeolite systems that include a binder [109].

Besides eliminating any trace of surface acidity, which would rapidly isomerize *para*-xylene back to an equilibrium mixture of xylenes, coke covers the vast majority of the pores, thereby increasing both the length of the crystal diffu-

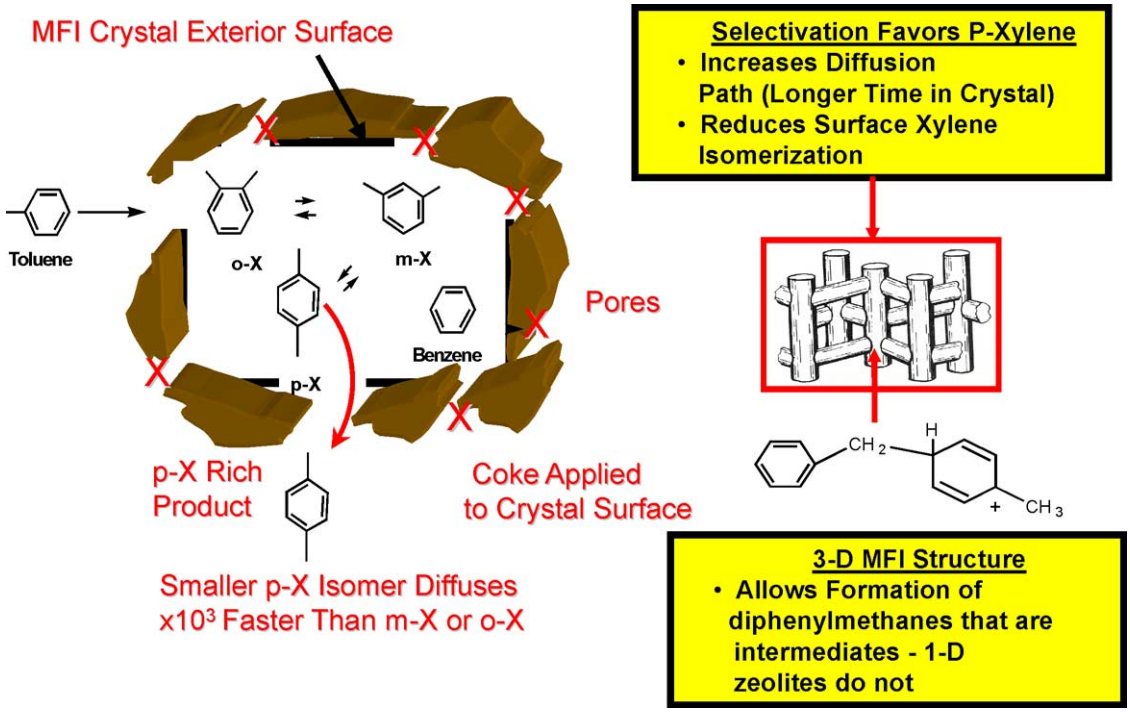

Fig. 7. Selectivation of the MFI crystal in the selective toluene disproportionation (STDP) process.

sion path and its tortuosity. The effect is to greatly increase the modulus and to reduce the effectiveness factor for *ortho*- and *meta*-xylene production. Because, as shown above, the diffusivity of *para*-xylene in MFI is significantly larger than that of *ortho*- or *meta*-xylene, the modulus for *para*-xylene production remains smaller and the effectiveness factor for toluene disproportionation is higher than that of xylene isomerization.

STDP is an excellent example of the application of shape selectivity to vastly exceed equilibrium yields of preferred products by playing off rates of diffusion vs rates of reaction.

10. Commercial processes that involve shape selective catalysis

STDP is one of more than 17 shape-selective processes that have been successfully commercialized. Tables 3 and 4 attempt to summarize commercial refining and petrochemical catalytic processes that are known to use shape-selective molecular sieves. The tables also attempt to identify which types of shape selectivity are operative. Missing is the MFI-catalyzed methanol-to-gasoline (MTG) process which was in commercial operation from 1985 until 1994. Additional examples of shape-selective reactions can be found in reviews by Venuto [11,12], Hoelderich et al. [110], Corma and Garcia [111], van der Waal and van Bekkum [112], and Song [113]. Venuto [11] has comprehensively reviewed organic chemistry involving zeolites. He discusses many mechanistic aspects not covered here. Obviously, there are many examples of shape-selective reactions that have been investigated at the laboratory and pilot plant scale, but most of these reactions lack the economic incentives needed for commercialization. Interestingly, the cost of catalyst development, even in the case of new framework structures, is rarely the key factor in whether the process reaches the commercial stage. Catalytic materials that appear to be expensive at the outset of a development program normally drop in cost as a result of economies of scale inherent in the raw materials and the materials synthesis.

11. Future opportunities for research and application of shape selectivity in molecular sieves

Along with the unresolved questions identified in the aforementioned studies, major opportunities exist for developing chiral-selective molecular sieves. The synthesis of pure enantiomers could be envisioned as the ultimate challenge in shape-selective catalysis. Beta (BEA) is one of the few molecular sieves thus far identified that exhibits chirality [132]. However, attempts to produce enantioselective products over BEA with high purity have been unsuccess-

Table 3
Catalytic shape selectivity in commercial refining processes

Refining process	Reaction	Zeolite or molecular sieve	Type of shape selectivity	How it is manifested	Ref.
FCC	Production of higher octane gasoline	MFI	RSS	Low-octane-number linear and monobranched olefins are isomerized; higher MW linear olefins with low octane numbers exit the gasoline pool via cracking	[114]
FCC	Production of low-MW olefins (especially propylene)	MFI	TSS	Prevents the formation of the transition state required for hydrogen transfer and prevents the formation of coke within the zeolite pores	[115]
Hydrocracking paraffins in distillate	Removal of higher melting point paraffins from diesel and heavy fuel oil fractions	MFI	RSS	Linear or near-linear paraffins with the highest melting points are removed by selective cracking in the pores of the zeolite	[116a]
Hydrocracking paraffins in lubricant raffinates	Removal of higher melting point paraffins from lubricant fractions	MFI	RSS	Linear or near-linear paraffins with the highest melting points are removed by selective cracking in the pores of the zeolite	[116b]
Hydroisomerization	Low octane C5 and C6 linear paraffins undergo skeletal isomerization to higher octane isoparaffins	MOR and MAZ (+ strong hydrogenation function)	PSS and PMKLS	Bulky isomers diffuse more easily out of the pores of larger 1-dimensional pore systems	[117]
Hydroisomerization	Higher melting point long-chain paraffins undergo skeletal isomerization to produce slightly branched paraffins with improved low-temperature viscosity	SAPO-11 and other shape selective molecular sieves (+ strong hydrogenation function)	TSS, PMKLS, and PSS	Preferential formation of 2- and 3-methyl paraffins near the pore mouth (TSS and perhaps key–lock selectivity); absence of isoalkanes containing adjacent methyl groups (TSS); preferred formation of 2- and 3-methyl alkanes through differences in rates of diffusion (PSS)	[118]

Table 4
Catalytic shape selectivity in commercial petrochemical processes

Petrochemical process	Reaction	Zeolite or molecular sieve	Type of shape selectivity	How it is manifested	Ref.
Xylene isomerization	Isomerize *ortho*- and *meta*-enriched xylene feeds and convert ethylbenzene to ethane and benzene or to additional xylenes	MFI, MOR, and other proprietary molecular sieves	TSS	In MFI, transalkylation to undesirable polymethyated (C_9^+) benzenes is precluded by steric constraints exerted by the pore walls. In MOR, the xylenes rapidly reach equilibrium because of the large number of acid sites. Higher activity of MOR allows lower temperature operation which reduces the selectivity for transalkylation in the less constrained pores of MOR.	[119]
Toluene disproportionation	Disproportionate toluene into benzene and either mixed xylenes (unselectivated zeolite) or *p*-xylene (selectivated zeolite)	MFI, MOR, and other proprietary molecular sieves	PSS (primary) and TSS (secondary) MTC?	Prevents formation of higher molecular weight C_9^+ polymethylbenzenes and facilitates the formation of diphenylmethyl intermediate.	[120]
Transalkylation of C_9^+ aromatics	Transalkylate toluene with methyl groups present in C_9^+ polymethylbenzenes	MOR and other proprietary large pore zeolites	TSS, RSS and PSS	Zeolite admits C_9 and C_{10} polymethylbenzenes, excludes higher molecular weight polymethylbenzenes, which could act as coke precursors, and precludes formation of polyphenyl compounds. C_8 aromatics rapidly diffuse out of the pore system.	[121]
Ethylbenzene synthesis	Benzene is alkylated with ethylene	MFI and MWW	TSS (primary) and PSS (secondary) in MFI; NE and TSS in MWW	Polyethylation is precluded by steric inhibition of *m*- and *p*-ethylbenzene. Ethylbenzene diffuses out of the pores at a much higher rate than any diethylbenzene that is formed.	[46,122]
para-Diethylbenzene synthesis	Benzene is alkylated with ethylene	MTW	TSS (primary) and PSS (secondary)	Prevents formation of higher molecular weight C_{11}^+ polyethylbenzenes and facilitates the formation of diphenylethyl intermediate.	[123]
Cumene synthesis	Benzene is alkylated with propylene	MWW and BEA	NE and TSS	Formation of di- and tripropylbenzenes is precluded by the steric costraints of the 12-MR surface pocket. Propylene oligomerization does not occur within the confines of the 12-MR pore.	[46,124]
Synthesis of linear alkylbenzenes	Long-chain linear olefins are reacted with benzene to form linear alkyl benzenes which are precursors for linear alkylbenzene sulfonate detergents	BEA, MWW, and other 12-MR zeolites	TSS	Polyalkylated benzenes are precluded from forming by the steric constraints provided by the 12-MR pores.	[125,126]
Olefin oligomerization	Propylene and *n*-butene are oligimerized to produce C_6^+ linear or near-linear olefins	MFI and other 10-MR zeolites	TSS	Polymethyl isoolefins and especially gem dimethyl olefins are precluded from forming by the steric constraints provided by the 10-MR pores.	[127]
Olefin skeletal isomerization	*n*-Butene and *n*-pentene are converted to iso-olefins as intermediates in the production of methyl *tert*-butyl ether (MTBE) and *tert*-amyl methyl ether (TAME)	FER, TON, and SAPO-11	TSS	C_4 dimer does not have sufficient room to form inside micropores and isomerization occurs through rearrangement of primary carbenium ion that is stabilized within the pores. Alternatively, *n*-butene is alkylated on benzylic ion formed near pore mouth followed by methy migration and β scission.	[128]
Pyridine synthesis	Ammonia, formaldehyde, and acetaldehyde are reacted to produce pyridine and α- and β-picoline	MFI	TSS and PSS	Mechanism still not well understood.	[129]

(*continued on next page*)

Table 4 (*Continued*)

Petrochemical process	Reaction	Zeolite or molecular sieve	Type of shape selectivity	How it is manifested	Ref.
Benzene synthesis from *n*-hexane	*n*-Hexane is converted to benzene via dehydrocyclization	LTL	TSS, NE?	*n*-Hexane adsorbs onto the walls of the LTL zeolite and is selectively adsorbed onto small Pt crystals within the LTL pores, where it undergoes dehydrocyclization.	[130]
Phenol hydroxylation and cyclohexanone ammoxidation	Selective oxidation of organic substrate using hydrogen peroxide as the oxidzing agent	TS-1	TSS and PSS	Hydrophobicity and isolation of titanium sites in molecular sieve are believed to play a part in shape-selective oxidation reactions.	[131]

ful. The potential commercial applications are vast. Chiral soluble acids and bases have been successfully used as catalysts, as have heterogeneous metallic catalysts modified with chiral "auxiliaries" such as tartrate-modified nickel and cinchona-modified platinum. However, chiral immobilized complexes have been more difficult to apply. The major challenge lies in the modification of existing molecular sieves with ligands that produce racemically pure fine chemicals. Zukal et al. [133], Darlt and Davis [132], and Davis [134] have studied this area of chiral zeolites.

Another opportunity area lies in the modification of mesoporous molecular sieves for shape-selective reactions involving larger molecules. Researchers have already functionalized the pores of mesoporous materials such as MCM-41 to selectively adsorb low concentrations of metals such as Hg and Ag while excluding other metals [135]. Metallocene catalysts have been successfully incorporated into the tubular pores of MCM-41 to produce crystalline nanofibers of polyethylene with diameters of 30 to 50 nm and molecular weights exceeding 6 million [136]. It remains to be seen whether the same approach could be used, for example, to produce isotactic or syndiotactic polypropylene.

There is also a substantial incentive to identify and develop shape-selective base catalysts for the synthesis of fine and intermediate chemicals [137]. There are only a few examples where modified molecular sieves have progressed past the laboratory stage for base-catalyzed reactions. One of these is the selective synthesis of 4-methylthiazome (4-MT) over Cs-exchanged ZSM-5 via the cyclization reaction involving isopropylidene methylidine and SO_2 [138]. Another is the transesterification of ethylene carbonate with methanol over potassium-exchanged zeolite A [139]. In the case of base catalysis the active site is located in the pores rather than in the framework and the framework acts to concentrate the reactants. Presumably the same types of shape selectivity apply, but the distribution of the active sites throughout the crystal may be more easily controlled. In these systems, the size of the cation and the location of the cations would likely have a significant effect on reactant and product diffusivity.

Recently, the area of inorganic molecular sieve membranes has received a significant level of attention [140]. While the initial objective is developing materials that separate small molecules under elevated temperatures or highly aggressive conditions where conventional polymeric membranes fail, a significant incentive exists for developing materials that combine reaction with separation. Shape selectivity and reaction can therefore be physically separated in a membrane, as in the selective hydrogenation of the permeate, by incorporation of a metal function only on the hydrogen-enriched side of the membrane [141].

Finally, the grand challenge in shape-selective catalysis is to utilize computational modeling to design the ideal molecular sieve for a specific targeted reaction using reaction transition state, intermediate size, and active site location as design parameters, and then to subsequently synthesize the molecular sieve in the laboratory. Designing molecular sieve "microreactors" that are tailor-made for a target reaction has been an elusive goal pursued by many synthetic chemists. Because the discovery of new frameworks is still to a large extent serendipitous, we will have to be satisfied with attempting to adopt the current, but ever-expanding set of molecular sieve crystal structures to particular reactions. The choice of a suitable framework and subsequent catalyst development effort will inevitably draw heavily on shape-selective theory, coupled with model compound tests and advanced materials characterization techniques, to produce the ideal catalyst for each targeted reaction.

12. Conclusions

Shape-selective catalysis is well accepted within the petroleum refining and petrochemical industries. While the field is over four decades old, it still remains an important source for new process concepts and improvements in current catalytic processes. Advances in computational modeling and major strides in materials characterization have helped to advance our understanding of how molecules interact with inorganic molecular sieves. Still, some gaps remain in our understanding. Despite these gaps, an appreciation of the basic underlying principles of shape selectivity combined with an intimate knowledge of the mechanism of the target catalytic reaction provides a high degree of confidence that one will be able to develop the optimum catalyst for the targeted application.

Acknowledgments

The author expresses his appreciation to Drs. Dominick N. Mazzone, Jeffrey S. Beck, and N.Y. Chen for many useful discussions on shape selectivity and shape selective catalysis and to ExxonMobil Research and Engineering for the opportunity to publish this work.

References

[1] P.B. Weisz, V.J. Frilette, J. Phys. Chem. 64 (1960) 382.
[2] P.B. Weisz, Chemtech 3 (1973) 498.
[3] P.B. Weisz, V.J. Frilette, R.W. Maatman, E.B. Mower, J. Catal. 1 (1962) 307.
[4] P.B. Weisz, Pure Appl. Chem. 52 (1980) 2091.
[5] P.B. Weisz, Ind. Eng. Chem. Res. 34 (1995) 2692.
[6] S.M. Csicsery, Stud. Surf. Sci. Catal. 94 (1995) 1.
[7] S.M. Csicsery, Pure Appl. Chem. 58 (1986) 841.
[8] S.M. Csicsery, Chem. Br. 21 (1985) 473.
[9] S.M. Csicsery, in: J.A. Rabo (Ed.), Zeolite Chemistry and Catalysis, in: ACS Monograph, Vol. 171, Am. Chem. Society, Washington, DC, 1976, p. 680.
[10] S.M. Csicsery, Zeolites 4 (1984) 202.
[11] P.B. Venuto, Micropor. Mater. 3 (1994) 297.
[12] P.B. Venuto, P.S. Landis, Adv. Catal. 18 (1968) 259.
[13] C. Song, J.M. Garces, Y. Sugi (Eds.), Shape-Selective Catalysis—Chemicals Synthesis and Hydrocarbon Processing, in: Am. Chem. Soc. Sympos. Ser., Vol. 738, Am. Chem. Society, Washington, DC, 1999.
[14] C.R. Marcilly, Top. Catal. 13 (2000) 357.
[15] F.G. Dwyer, Stud. Surf. Sci. Catal. 67 (1991) 179.
[16] W.O. Haag, Stud. Surf. Sci. Catal. 84 (1994) 1375.
[17] N.Y. Chen, T.F. Degnan, C.M. Smith, in: Molecular Transport and Reaction in Zeolites, VCH, New York, 1994, p. 309.
[18] N.Y. Chen, W.E. Garwood, Catal. Rev. Sci. Eng. 28 (1986) 185.
[19] N.Y. Chen, W.E. Garwood, F.G. Dwyer, in: Shape Selective Catalysis in Industrial Applications, 2nd ed., Dekker, New York, 1996, p. 282.
[20] P.B. Weisz, Erdol Kohle 18 (1965) 527.
[21] C.D. Chang, in: Hydrocarbons from Methanol, Dekker, New York, 1983, p. 24.
[22] J.S. Buchanan, Catal. Today 55 (2000) 207.
[23] D.S. Santilli, T.V. Harris, S.I. Zones, Micropor. Mater. 1 (1993) 329.
[24] M. Schenk, S. Calero, T.L.M. Maesen, L.L. van Benthem, M.G. Verbeek, B. Smit, Angew. Chem. Int. Ed. 41 (2002) 2500.
[25] R. Krishna, B. Smit, Chem. Innovation 31 (2001) 27.
[26] E.G. Derouane, Z. Gabelica, J. Catal. 65 (1980) 486.
[27] E.G. Derouane, Catalysis by Zeolites Stud. Surf. Sci. Catal. 5 (1980) 5.
[28] S.J. Miller, Micropor. Mater. 2 (1994) 439.
[29] J.M. Campelo, F. Lafont, J.M. Marinas, U. Cordoba, J. Catal. 156 (1995) 11.
[30] J.A. Martens, R.F. Parton, L. Uytterhoeven, P.A. Jacobs, Appl. Catal. 76 (1991) 95.
[31] J.A. Martens, W. Souverijns, W. Verrelst, R.F. Parton, G.F. Froment, P.A. Jacobs, Angew. Chem. Int. Ed. 34 (1995) 2528.
[32] W. Souverijns, G.F. Froment, J.A. Martens, L. Uytterhoeven, P.A. Jacobs, Stud. Surf. Sci. Catal. B 105 (1997) 1285.
[33] W. Souverijns, J.A. Martens, G.F. Froment, P.A. Jacobs, J. Catal. 174 (1998) 177.
[34] J.A. Martens, G. Vanbutsele, P.A. Jacobs, J. Denayer, R. Ocakoglu, G. Baron, J.A. Munoz Arroyo, J. Thybaut, G.B. Marin, Catal. Today 65 (2001) 111.
[35] J.A. Munoz Arroyo, G.G. Martens, G.F. Froment, G.B. Marin, P.A. Jacobs, J.A. Martens, Appl. Catal. A Gen. 192 (2000) 9.
[36] M.C. Claude, J.A. Martens, J. Catal. 190 (2000) 39.
[37] R.L. Gorring, J. Catal. 31 (1973) 13.
[38] R.L. Gorring, R.J. Daniels, ACS Sympos. Ser. 248 (1984) 51.
[39] E. Ruckenstein, P.S. Lee, Phys. Lett. A 56 (1976) 423.
[40] J.M. Nitsche, J. Wei, AIChE J. 37 (1991) 661.
[41] N.Y. Chen, S.J. Lucki, E.B. Mower, J. Catal. 13 (1969) 329.
[42] J.P. Gianetti, A.J. Perotta, Ind. Eng. Chem. Proc. Des. Dev. 14 (1975) 86.
[43] M. Schenk, B. Smit, T.J.H. Vlugt, T.I.L.M. Maesen, Angew. Chem. Int. Ed. 40 (2001) 736.
[44] D. Fraenkel, M. Cherniavsky, M. Levy, in: Proc. 8th Intern. Congr. Catal., Vol. 4, 1984, p. 545.
[45] E.G. Derouane, Z. Gabelica, J. Catal. 65 (1980) 486.
[46] T.F. Degnan, C.M. Smith, C.R. Venkat, Appl. Catal. A 221 (2001) 283.
[47] C.B. Khouw, M.E. Davis, Am. Chem. Soc. Sympos. Ser. 517 (1993) 206.
[48] D.S. Santilli, S.I. Zones, Catal. Lett. 7 (1990) 383.
[49] P.B. Weisz, Faraday Disc. Chem. Soc. 72 (1981) 374.
[50] J.P. Gilson, E.G. Derouane, J. Catal. 88 (1984) 538.
[51] D.S. Shihabi, W.E. Garwood, P. Chu, J.N. Miale, R.M. Lago, C.T.-W. Chu, C.D. Chang, J. Catal. 93 (1985) 471.
[52] US Patent 4,173,622 [assigned to FMC Corp.], November 6, 1979.
[53] US Patent H191 [assigned to W.R. Grace], January 6, 1987.
[54] US Patent 5,401,704 [assigned to Mobil Oil], March 28, 1995.
[55] US Patent 5,620,590 [assigned to Mobil Oil], April 15, 1997.
[56] M. Farcasiu, T.F. Degnan, Ind. Eng. Chem. Res. 27 (1988) 45.
[57] C. Song, X. Ma, H.H. Schobert, in: Shape-Selective Catalysis—Chemicals Synthesis and Hydrocarbon Processing, in: Am. Chem. Soc. Sympos. Ser., Vol. 738, Am. Chem. Society, Washington, DC, 1999, p. 305.
[58] J.H. Sinfelt, Surf. Sci. 500 (2002) 923.
[59] J. Weitkamp, S. Ernst, Catal. Today 19 (1994) 107.
[60] R. Millini, G. Perego, J.W.O. Parker, G. Bellussi, L. Carluccio, Micropor. Mater. 4 (1995) 221.
[61] G. Bellussi, G. Pazzuconi, C. Perego, G. Girotti, G. Terzoni, J. Catal. 157 (1995) 227.
[62] G. Bellussi, G. Perego, M.G. Clerici, A. Giusti, Eur. Patent 293,032, 1988.
[63] C. Perego, S. Aarilli, R. Millini, G. Bellussi, G. Girotti, G. Terzoni, Micropor. Mater. 6 (1996) 395.
[64] M.E. Leonowicz, J.A. Lawton, S.L. Lawton, M.K. Rubin, Science 264 (1994) 1910.
[65] J.C. Cheng, T.F. Degnan, J.S. Beck, Y.Y. Huang, M. Kalyanaraman, J.A. Kowalski, C.A. Loehr, D.N. Mazzone, in: Science and Technology in Catalysis, TOCAT-3, Kodansha (1998), 1999, p. 53.
[66] J.A. Horsley, Chemtech 10 (1997) 45.
[67] H.H. Mooiweer, K.P. de Jong, B. Kraushaar-Czarnetzki, W.H.J. Stork, B.C.H. Krutzen, Stud. Surf. Sci. Catal. 84 (1994) 2327.
[68] A.W. Chester, P. Chu, W.J. Rohrbaugh, Presented at the 10th North American Catal. Soc. Mtg., San Diego, CA (May 17–22, 1987).
[69] W.O. Haag, R.M. Lago, P.B. Weisz, Faraday Discuss. Chem. Soc. 72 (1981) 317.
[70] A. Wheeler, Adv. Catal. 3 (1951) 249.
[71] D.M. Ruthven, Can. J. Chem. 52 (1974) 3523.
[72] M. Buelow, H. Schlodder, P. Struve, Adsorb. Sci. Technol. 3 (1986) 229.
[73] J. Wei, J. Catal. 75 (1982) 433.
[74] W.T. Mo, J. Wei, Chem. Eng. Sci. 41 (1986) 703.
[75] D.H. Olson, W.O. Haag, ACS Sympos. Ser. 248 (1984) 275.
[76] L.B. Young, S.A. Butter, W.W. Kaeding, J. Catal. 76 (1982) 418.
[77] C.W. Jones, M.E. Davis, Nature 393 (1998) 52.
[78] M. Niwa, T. Kunieda, J.-H. Kim, in: Shape-Selective Catalysis—Chemicals Synthesis and Hydrocarbon Processing, in: Am. Chem. Soc. Sympos. Ser., Vol. 738, Am. Chem. Society, Washington, DC, 1999, p. 181.
[79] V.J. Frilette, W.O. Haag, R.M. Lago, J. Catal. 67 (1981) 218.

[80] J. Weitkamp, S. Ernst, C.Y. Chen, Stud. Surf. Sci. Catal. 49 (1989) 1115.
[81] H. Dauns, J. Weitamp, Chem. Ing. Technol. 11 (1986) 900.
[82] S.M. Csicsery, J. Catal. 108 (1987) 433.
[83] J. Weitkamp, C.Y. Chen, S. Ernst, in: T. Inui (Ed.), Successful Design of Catalysts, Elsevier, Amsterdam, 1988, p. 343.
[84] J. Weitkamp, S. Ernst, C.Y. Chen, in: P.A. Jacobs, R.A. van Santen (Eds.), Zeolites: Facts, Figures, Future, Proc. 8th Int. Zeolite Conf., Amsterdam (July 10–14, 1989), Elsevier, Amsterdam, 1989, p. 1115.
[85] S.I. Zones, T.V. Harris, Micropor. Mesopor. Mater. 35 (2000) 31.
[86] J.M. Thomas, G.R. Millward, S. Ramdas, L.A. Bursill, M. Audier, Faraday Discuss. Chem. Soc. 72 (1981) 345.
[87] E.G. Derouane, P. Dejaifve, Z. Gableica, J. Vedrine, Faraday Discuss. Chem. Soc. 72 (1981) 331.
[88] Y. Okamoto, N. Oshima, Y. Kobayashi, O. Terasaki, T. Kodaira, T. Kubota, Phys. Chem. Chem. Phys. 4 (2002) 2852.
[89] O. Terasaki, T. Ohsuna, S. Inagaki, Catal. Sur. Jpn. 4 (2000) 99.
[90] P. Wagner, Phys. Chem. 103 (1999) 8245.
[91] S. Inagaki, J. Am. Chem. Soc. 121 (1999) 9611.
[92] A. Carlsson, J. Electron Microsc. 48 (1999) 795.
[93] Y. Sakamoto, M. Kaneda, O. Terasaki, D.Y. Zhao, J.M. Kim, G. Stucky, H.J. Shin, R. Ryoo, Nature 408 (2000) 449.
[94] T. Ohsuna, Y. Horikawa, K. Hiraga, O. Terasaki, Chem. Mater. 10 (1998) 688.
[95] M.W. Anderson, J.R. Agger, N. Hanif, O. Terasaki, T. Ohsuna, Solid State Phys. 3 (2001) 809.
[96] M.W. Anderson, Curr. Opin. Solid State Mater. Sci. 5 (2001) 407.
[97] S.M. Holmes, C. Markert, R.J. Plaisted, J.O. Forrest, J.R. Agger, M.W. Anderson, C.S. Cundy, J. Dwyer, Chem. Mater. 11 (1999) 3329.
[98] C.A. Fyfe, Z. Altenschildesche, H. Meyer, K.C. Wong-Moon, H. Grondey, J.M. Chezeau, Solid State Nucl. Magn. Reson. 9 (1997) 97.
[99] H. Morell, K. Angermund, A.R. Lewis, D.H. Brouwer, C.A. Fyfe, H. Gies, Chem. Mater. 14 (2002) 2192.
[100] C.A. Fyfe, A.C. Diaz, J. Phys. Chem. 106 (2002) 2261.
[101] C.A. Fyfe, J.L. Bretherton, L.Y. Lam, J. Am. Chem. Soc. 123 (2001) 5285.
[102] M. Falconi, M.W. Deem, J. Chem. Phys. 110 (1999) 1754.
[103] R.W. Grosse-Kunstleve, L.B. McCusker, C. Baerlocher, J. Appl. Crystallogr. 30 (1997) 985.
[104] L.B. McCusker, C. Baerlocher, R. Grosse-Kunstleve, S. Brenner, T. Wessels, CHIMA 55 (2001) 497.
[105] P.C. Mihindou-Koumba, H.S. Cerqueira, P. Magnoux, M. Guisnet, Ind. Eng. Chem. Res. 40 (2001) 1042.
[106] P. Magnoux, H.S. Cerqueira, M. Guisnet, Appl. Catal. A 235 (2002) 93.
[107] D. Meloni, D. Martin, P. Ayrault, M. Guisnet, Catal. Lett. 71 (2001) 213.
[108] D. Meloni, D. Martin, M. Guisnet, Appl. Catal. A 215 (2001) 67.
[109] M. Misk, G. Joly, P. Magnoux, M. Guisnet, S. Jullian, Micropor. Mesopor. Mater. 40 (2000) 197.
[110] W. Hoelderich, M. Hesse, F. Naumann, Angew. Chem. Int. Ed. Engl. 27 (1988) 226.
[111] A. Corma, H. Garcia, Catal. Today 38 (1997) 257.
[112] J.C. Van der Waal, H. van Bekkum, J. Por. Mater. 5 (1998) 289.
[113] C. Song, Stud. Surf. Sci. Catal. 113 (1998) 163.
[114] F.G. Dwyer, T.F. Degnan, in: J. Magee (Ed.), Fluid Catalytic Cracking, Elsevier, 1993, Chap. 4.
[115] T.F. Degnan, G.K. Chitnis, P.H. Schipper, Micropor. Mesopor. Mater. 35–36 (2000) 245.
[116] (a) N.Y. Chen, R.L. Gorring, H.R. Ireland, T.R. Stein, Oil Gas J. 75 (1977) 165;
(b) K.W. Smith, W.C. Starr, N.Y. Chen, Oil Gas J. 78 (1980) 75.
[117] P.J. Kurchar, J.C. Bricker, M.E. Reno, R.S. Haizmann, Fuel Proc. Technol. 35 (1993) 183.
[118] C.R. Marcilly, Top. Catal. 13 (2000) 357.
[119] S. Bhatia, Zeolite Catalysis: Principles and Applications, CRC Press, Boca Raton, FL, 1990.
[120] T.C. Tsai, S.B. Liu, I. Wang, Appl. Catal. A 181 (1999) 355.
[121] Eur. Patent 731071 A, 1996.
[122] D.N. Mazzone, C.R. Venkat, P.J. Lewis, B.R. Maerz, Hydrocarbon Asia 3 (1997) 56.
[123] F.G. Dwyer, S. Ram, in: AIChE Spring Nat. Mtg., Houston, TX (April 7–11, 1991), 1991.
[124] M.F. Bentham, G.J. Gadja, R.H. Jensen, H.A. Zinner, Erdoel Erdgas Kohle 113 (1997) 84.
[125] A. Keshavaraja, K.R. Srinivasan, Chem. Ind. Dig. 8 (1995) 127.
[126] J.L.G. de Almeida, M. Dufaux, Y. Ben Tarit, C. Naccache, J. Am. Oil Chem. Soc. 71 (1994) 675.
[127] S. Yurchak, J.E. Child, J.H. Beech, in: NPRA Annual Meeting, San Antonio, TX (March 25–27, 1990), 1990, Paper AM-90-37.
[128] Chem. Week, March 25, 1992, p. 9.
[129] Y.S. Higasio, T. Shoji, Appl. Catal. A 221 (2001) 197.
[130] Chem. Week, February 12, 1997, p. 20.
[131] C. Perego, A. Carati, P. Ingallina, M.A. Mantegazza, G. Bellussi, Appl. Catal. A 221 (2001) 63.
[132] C.B. Dartt, M.E. Davis, Ind. Eng. Chem. Res. 33 (1994) 2887.
[133] A. Zukal, V. Patzelova, N. Lohse, Zeolites 6 (1986) 133.
[134] M.E. Davis, C&E News 79 (13) (2001) 96.
[135] X. Feng, G.E. Fryxell, L.Q. Wang, A.Y. Kim, J. Liu, K.M. Kemner, Science 276 (1997) 923.
[136] K. Kageyama, J. Tamazawa, T. Aida, Science 285 (1999) 2113.
[137] J.C. Kim, H.X. Li, M.E. Davis, Prepr. ACS 206 (August 22, 1993).
[138] US Patent 5,231,187 [issued to Merck], July 27, 1993.
[139] D. Delledonne, F. Rivetti, U. Romano, Appl. Catal. A Gen. 221 (2001) 241.
[140] J. Caro, M. Noack, P. Kolsch, R. Schafer, Micropor. Mesopor. Mater. 38 (2000) 3.
[141] G. Saracco, V. Specchia, Catal. Rev. Sci. Eng. 36 (1994) 105.